Triacylglycerol structures and the chocolate fat bloom mechanism

van Mechelen, J.B.

Chapter 5

Structures of mono-unsaturated triacylglycerols

Part IV

The highest melting *β′*-2 polymorphs of *trans*-mono-unsaturated triacylglycerols and related saturated TAGs and their polymorphic stability

based on *Acta Cryst.* (2008) B**64**, 249-259.

5.1 Abstract

The β'_1-2 crystal structures of a series of mixed-chain saturated and *trans*-mono-unsaturated triacylglycerols containing palmitoyl, stearoyl and elaidoyl acyl chains have been solved from high-resolution powder diffraction data, from synchrotron as well as laboratory X-ray sources. The structures crystallized in space group *I*2 with two independent molecules forming a dimer in the asymmetric unit, and packed in double-chain length layers. In contrast to the β-2 structures of these and similar types of TAGs, the molecular conformations of β'_1-2 symmetric and β'_1-2 asymmetric mixed triacylglycerols are different, although both types have the *sn*-2 chain in a leg position of the chair-shaped conformation. A transformation to the β-2 structure with the *sn*-2 chain in the back position is complicated and unlikely to take place in the solid state. A novel β'-2 polymorph of PSS has been crystallized and its structure has been solved. The melting point (339 K) of this so-called β'_0-2 polymorph is 2 K above that of the β'_1-2 polymorph and almost equal to that of the β-2 polymorph of PSS. The difference in packing of the β'_0-2 *versus* β'_1-2 explains the slow β'_1-2 to β'_0-2 phase transition. The transition is strikingly similar to the β_2-3 to β_1-3 transition in *cis*-mono-unsaturated triacylglycerols.

5.2 Introduction

Fat blends are used as shortenings in bakery products and in table spreads to provide these products with the appropriate stability, firmness, and melting and crystallization properties. For most applications the mixture of triacylglycerols (TAGs) in the fat blends should be in the β' polymorph. The β' phase crystallites are small, have a needle-like crystal habit and tend to aggregate into a network, in which air and liquid components are better stabilized than by the larger β phase crystallites. As a result, the β' phase provides a smooth feel in the mouth (Wiedermann, 1978; Ghotra *et al*., 2002). Stability of the β' phase is important and phase segregation or a transition to the β phase should be avoided because of deterioration of the quality of the product. For example, the problem of graininess in margarines due to the occurrence of β-phase crystallites is well known (Watanabe *et al*., 1992)

Most vegetable oils are too soft to be applied as such in the above-mentioned consumer products. They need modification, *e.g. via* fractionation of the natural product (Timms, 2005; Kellens *et al.*, 2007) or interesterification with other, harder types of fat (Sreenivasan, 1978). A third option is (partial) hydrogenation of the *cis* double bonds that are present in mono-unsaturated oleic-

acid chains (*cis*-9-octadecenoic acid; O; one of the most abundant unsaturated fatty-acid chains in natural fats and oils), and other polyunsaturated fatty-acid groups. For example, palm oil and low-melting palm-oil fractions such as palm olein contain large amounts of PPO (palmitic-acid, hexadecanoic acid: P), POO and POP. These oil components may be a starting source for the production of β'-stable PSP [stearic-acid, octadecanoic acid: S], PPS and PSS [c].

Although (partial) hydrogenation reduces the degree of unsaturation, increases the melting point and provides an improved stability against oxidation, it allows also the isomerization of the *cis* double bond into the *trans* isomer, *e.g.* the oleic fatty-acid chain becomes its *trans* isomer, elaidic acid (*trans*-9-octadecenoic acid; E). An overwhelming amount of research has been carried out to assess potential health hazards of these *trans* fatty acids because of their suspected competition with essential fatty acids (Valenzuela & Margado, 1999). Generally this research has led to the opinion that *trans* fatty acids hold certain health risks, resulting in a strong tendency to reduce their amount in food products.

Elaidoyl containing TAGs such as PEP and PPE are commonly believed to be structurally similar to their fully saturated analogues, PSP and PPS, respectively, although very little is known about their actual packing. Fully saturated and *trans*-mono-unsaturated TAGs can crystallize in various polymorphs, with melting points that usually increase in the order α, β'_2, β'_1 and β, but occurrence and stability of polymorphs depend on the precise fatty-acid composition of the TAGs. The existence of both β'_2-2 and β'_1-2 has been reported for PSP (Gibon *et al.*, 1985) as well as for the *trans*-mono-unsaturated TAGs PEP and PPE (Elisabettini *et al.*, 1998), while for PSS and PPS only the higher melting β'_1-2 has been reported (Lutton *et al.*, 1948; Lutton, 1950).

Conformational and packing differences influence the polymorphic stability and phase-transition behavior of the various TAGs. To obtain a better understanding of these processes, we used DSC and time-resolved X-ray powder diffraction (XRPD) together with crystal-structure determination from XRPD data. We found evidence for the existence of the lower melting β'_2-2 for PSP and PSS from the diffraction data and discovered a novel β' polymorph of PSS, coined β'_0-2, that melts higher than the β'_1-2 polymorph. In addition to the crystal structure of this novel β'_0-2 polymorph of PSS, we also present the crystal structures of the β'_1-2 polymorphs of PEP, PPE, PSP and PPS.

The structures will be analysed in terms of their methyl end-plane packing, and compared with the β-2 phase structures of these and similar TAGs that have been reported in Part III of this series (van Mechelen *et al.*, 2008) and a few β'-type crystal structures of TAGs that were solved earlier: CLC (single crystal), MPM (powder, van Langevelde *et al.*, 2000) and PPM (single crystal, Sato *et al.*, 2001).

[c] Carbon chain lengths are represented by the acronyms S: C18, P: C16 and E: C18:1 (*trans-9*), respectively.

5.3 Experimental

5.3.1 Samples, sample preparation and data collection

Samples of PEP and PPE have been obtained from Larodan Fine Chemicals AB (Malmö, Sweden). Molten sample material was placed into a capillary and crystallized. To increase the crystallite size samples have been annealed at a temperature just below their highest melting point (β'_1 polymorph) for a few minutes. The samples of PSP, PPS and PSS have been obtained from Unilever Research Laboratories (Vlaardingen, The Netherlands). The PSP sample was delivered as a β'_1–phase powder and measured as such in a glass capillary. Samples of PPS as well as PSS have been crystallized from the melt in a glass capillary. The formation of the β'_1 phase in PPS was stimulated by heating the sample just above the β'_2 to β'_1 conversion temperature. In case of PSS this procedure delivered initially a β'_1 polymorph that transformed into a novel β'–type polymorph after storage in the lab for several weeks.

For PEP, PPE, PSS and PPS XRPD data for structure solution have been collected at room temperature (298 K) at an X'pert Pro MPD diffractometer, equipped with a sealed Cu X-ray tube, a hybrid monochromator, primary and secondary soller slits with 0.01 rad divergence and an X'celerator strip detector (PANalytical, Almelo, The Netherlands). The continuous scans were binned with a step size of 0.008 °2θ. High-resolution synchrotron powder (HR-SPD) data of PSP were collected at the synchrotron beam line BM01b at the ESRF (Grenoble, France) at 250 K. The continuous scans were binned with a step size of 0.005 °2θ. During the data collection of PSP, the temperature at the capillary was controlled with an Oxford Instruments Cryostream (Abingdon, England), mounted with the temperature-controlled N_2 gas stream perpendicular to the capillary. This limited the temperature-controlled length of the capillary to 4 mm.

To determine the melting points (T_m) of the polymorphs and the phase-transition points, time- and temperature-resolved XRPD experiments were carried out using an X'pert Pro MPD instrument with an elliptical mirror, primary and secondary soller slits with 0.02 rad divergence, an X'celerator strip detector and an Oxford Instruments Cryostream Compact for temperature control. The latter was mounted with the temperature-controlled N_2 gas stream being parallel to the capillary and with an X-ray transparent cylindrical polymer film guiding the stream along the capillary. The capillary samples were heated with 0.5 K min^{-1} and the diffraction pattern was monitored continuously in 1 min scans from 0.5-30 °2θ with a step size of 0.016 °2θ. Capillaries were spun continuously in all experiments. Melting and phase-transition temperatures were determined by

quenching (-30 K min^{-1}) a seed-free melt from ~ 10 K above the melting point of the most stable (β') polymorph to 253 K so that the α phase crystallizes. Subsequently, the sample was heated slowly at 0.5 K min^{-1} and simultaneously the diffraction pattern was recorded with a time resolution of one minute. This protocol shows the development of the polymorphs: α transforms into β'_2, β'_2 transforms into β'_1 and, finally, heating of the β'_1 ends in a melt. It should be noted that for symmetric TAGs (PEP, PSP) a β-2 polymorph exists but this polymorph is difficult or even impossible to obtain from the melt (Chapter 4, van Mechelen *et al*., 2008) and for the asymmetric TAGs (PPE, PPS, PSS) the time scale of the experiment is too short to obtain the slow growing β-2 polymorph before T_m (β-2) is reached.

Phase transitions were analysed with DSC using a Linkam DSC600 instrument (Linkam Scientific Instruments Ltd, Tadworth, England). Samples were heated at 0.5 K min^{-1} and quenched at -30 K min^{-1}. Although the β'_2 to β'_1 transition process is clearly visible with our time-resolved XRPD equipment, it is not easy to trace with DSC using the same temperature profile.

Phase-transition points and melting points are listed in Table 5.1. The T_m of β'_0-2 of PSS has been determined in a separate XRPD run with β'_0 as starting phase.

Table 5.1 Phase transition (T in K) and melting points (T_m in K) of polymorphs of PEP, PSP, PPE, PPS and PSS.

TAG	T α to β'_2-2	T β'_2-2 to β'_1-2	T_m β'_1-2	T_m β'_0-2	T_m β-2
PEP	303	312	329	-	327
PSP	317	319	343	-	339.5
PPE	304	311	320	-	320
PPS	321	323	332	-	338
PSS	323	330	337	339	339

5.3.2 Indexing, model building, structure determination and refinement

As already explained in other publications (van Mechelen *et al*., 2006a, 2006b), indexing of TAG powder diffraction patterns is not straightforward because of dominant low-angle and higher-angle zones. The program *McMaille* (Le Bail, 2004) can generate a list of cell suggestions provided the search space is limited by applying restrictions to the allowed cell dimensions. With help of the program *Chekcell* (Laugier & Bochu, 2001) a further selection and cell refinement

can be carried out. Eventually this led to the monoclinic and orthorhombic unit cells that enabled the solution of the β'-2 structures.

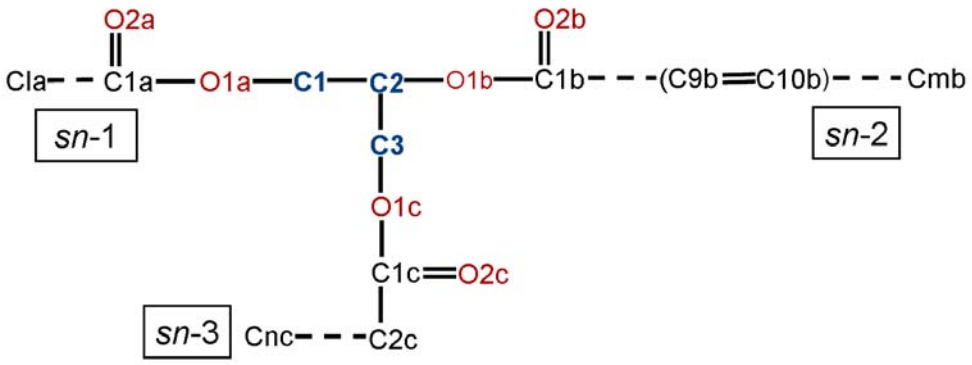

Fig. 5.1 Schematic drawing of a TAG molecule in the [1-3] conformation with *l*, *n* and *m* denoting the length of the acyl chains. The double bond has been drawn in the *sn*-2 chain but, if present, may also be located in one of the other chains.

The TAGs discussed in this paper all crystallize in a chair-shaped conformation (Fig. 5.1). The positions of the three *sn*-acyl chains, numbered 1, 2, 3 from left to right in the three-character TAG acronyms, may differ from TAG to TAG and therefore a numerical identifier [x-y] is used to discriminate the conformations. In the notation [*x*-*y*] the '*x*' is the *sn* chain (number) that is in the chair's back-leg position and the '*y*' the *sn* chain that forms the seat plus front-leg position. For symmetric molecules, such as PEP and PSP, a [1-2] conformation is equivalent to a [3-2] conformation but for asymmetric molecules, such as PPE and PPS, the presence of the longer chain at either the back or at the seat/front leg position, *e.g.* [2-1] PPE *versus* [2-3] PPE respectively, imply different structural models with potentially different types of packings.

Fig. 5.2 shows the diffraction patterns of the β' structures. The pattern of β'-PSP has been rescaled to Cu $K\alpha_1$ radiation to simplify the comparison with the other patterns. The lowest-angle observed reflection in all the patterns (d-spacing ~ 43-44 Å) is indicative of a double-chain length packing and is denoted by addition of '-2' to the polymorph name.

For the structure solution of the β'-2 structures with *FOX* (Favre-Nicolin & Cerný, 2002) a starting model with a [1-2] conformation was built in a *Z*-matrix description. At the start-up of the structure-solution process (parallel tempering) rigid molecular models were used with translational and rotational freedom only. In the course of the structure-solution process, only torsion angles around the central glycerol moiety were released, one by one.

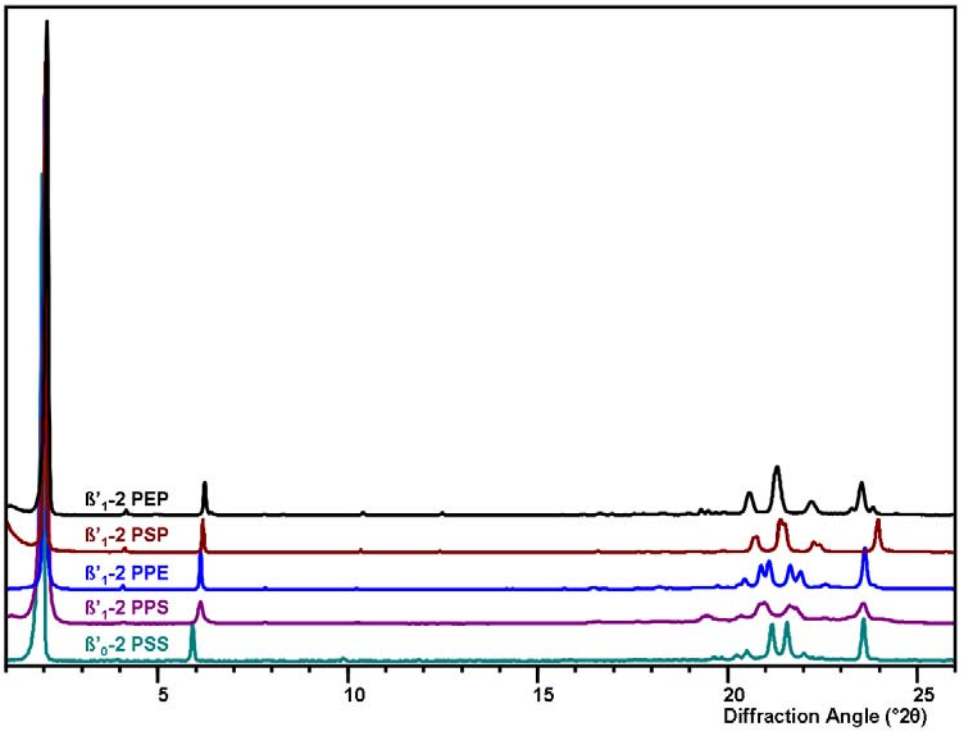

Fig. 5.2 β'-2 diffraction patterns of PEP, PSP, PPE, PPS and PSS with PSP rescaled to Cu $K\alpha_1$.

Structure refinement was carried out with the program *GSAS* (Larson & Von Dreele, 1987). The background was modelled by a Chebyshev polynomial. By using profile function 4 (*hkl*)-dependent peak broadening as well as low-angle peak asymmetry was taken into account. Soft restraints were applied to all the distances and angles. Soft planar restraints were applied to the saturated acyl chains (S, P) in the legs and the back of the chair-shaped molecules. Planar restraints were also applied to the carbon acyl chains at either side of the *trans* double bond in the E-chain. Atomic displacement parameters have not been refined. Correction for preferred orientation ([001] as direction) with the March-Dollase function (March, 1932; Dollase, 1986) in the final state of the refinement affected the R values only slightly. A summary of the results of the Rietveld refinements is listed in Table 5.2. Figures of the full traces of all diffraction patterns including the difference trace from the Rietveld refinement are shown in Figs. 5.11-5.15 (§5.8 Appendix).

Table 5.2 Summary of the results of Rietveld refinement

	[1-2]β'_1-2 PEP	[1-2]β'_1-2 PSP	[2-3]β'_1-2 PPE	[2-3]β'_1-2 PPS	[1-2]β'_0-2 PSS
Chemical form	$C_{53}H_{100}O_6$	$C_{53}H_{102}O_6$	$C_{53}H_{100}O_6$	$C_{53}H_{102}O_6$	$C_{55}H_{106}O_6$
M_r	833.38	835.39	833.38	835.39	863.45
Cell setting space group	Monoclinic *I*2	Monoclinic *I*2	Monoclinic *I*2	Monoclinic *I*2	Monoclinic *C*2/*c*
$T_{\text{data coll.}}$ (K)	293	250	298	297	297
a, *b*, *c* (Å)	22.715 (5) 5.656 (2) 85.110 (4)	22.253 (3) 5.634 (1) 85.263 (4)	22.99 (2) 5.641 (5) 86.265 (7)	22.75 (1) 5.650 (5) 86.746 (5)	22.651 (6) 5.653 (3) 89.462 (4)
β (°)	90.20 (1)	90.80 (3)	93.52 (12)	93.968 (11)	90.01 (6)
V (Å^3)	10934.0 (6)	10688.6 (6)	11164.5 (9)	11123.2 (9)	11455.5 (8)
Z (Z')[d]	8 (2)	8 (2)	8 (2)	8 (2)	8 (1)
D_x (Mg m^{-3})	1.01	1.04	0.99	1.00	1.00
Radiation type	Cu $K\alpha_1$	Synchrotron	Cu $K\alpha_1$	Cu $K\alpha_1$	Cu $K\alpha_1$
Specimen form, colour	Solid fat, white	Solid fat, white	Solid fat, white	Solid fat, white	Solid fat, white
Specimen size (mm)	12 × 1 × 1	4 × 1.5 × 1.5	12 × 0.7 × 0.7	12 × 0.7 × 0.7	12 × 0.7 × 0.7
Diffractometer	Xpert-Pro	BM01b ESRF	Xpert-Pro	Xpert-Pro	Xpert-Pro
2θ (°) range	0.8 - 40	0.14 - 35.5	0.8 - 45	0.8 - 40	0.8 - 45
R factors and goodness-of-fit	R_p = 0.061 R_{wp} = 0.086 R_{exp} = 0.019 S = 4.89	R_p = 0.059 R_{wp} = 0.070 R_{exp} = 0.022 S = 3.35	R_p = 0.064 R_{wp} = 0.095 R_{exp} = 0.041 S = 3.40	R_p = 0.060 R_{wp} = 0.090 R_{exp} = 0.034 S = 2.78	R_p = 0.069 R_{wp} = 0.106 R_{exp} = 0.037 S = 3.09
λ (Å)	1.54059	0.79948	1.54059	1.54059	1.54059
No. of parameters	986	1005	985	996	540

[d] Z = number of molecules in unit cell; Z' = number of molecules in asymmetric unit

5.4 Results and discussion

5.4.1 The structure determination process

5.4.1.1 β'_1-2 PEP, β'_1-2 PSP, β'_1-2 PPE and β'_1-2 PPS

The patterns of β'_1-2 PEP, β'_1-2 PSP, β'_1-2 PPE and β'_1-2 PPS could be indexed as monoclinic with eight molecules in the unit cell in view of the expected density of ~ 1.0 g cm^{-3}. The lower-angle part of the fingerprint area of these patterns is dominated by the reflections (31ℓ) (ℓ = even) while the (31ℓ) (ℓ = odd) are absent (Fig. 5.3). Also the (00ℓ) (ℓ = odd) are absent, but no other systematic absences are detectable, implying *I*1-1 or the non-standard (and related) *A*1-1 as possible extinction symbols. Structure determination runs with mirror-plane-

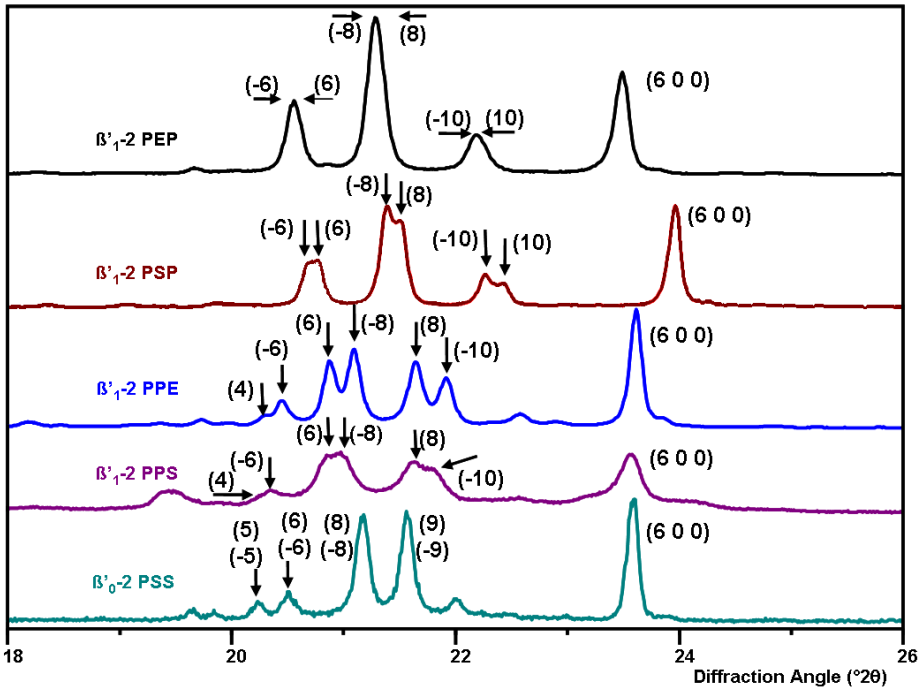

Fig. 5.3 Fingerprint area of the β'-2 diffraction patterns of PEP, PSP, PPE, PPS and PSS with PSP rescaled to Cu $K\alpha_1$. Peaks are marked with Miller indices. From the (31ℓ) reflections (between 20 and 23 °2θ) only the ℓ is given.

containing space groups were not successful, leaving *I*2 (and *A*2) as the possible space group option(s), with two independent molecules in the asymmetric unit.

Fig. 5.3 shows that the (31ℓ) reflections of β'_1-2 PEP and β'_1-2 PSP are grouped in pairs with opposite signs for the ℓ-values. This pairing also occurs in β'_1-2 PPE and β'_1-2 PPS but with unequal ℓ values. With the program *Chekcell* an alternative indexing in space group *A*2 was found for β'_1-2 PPE and β'_1-2 PPS with pairs of equal ℓ values with opposite sign while keeping the (600) at its position. In this alternative *A*2 cell for β'_1-2 PPE as well as β'_1-2 PPS [2-3] models could be refined to quite acceptable R_p values, just above (~1%) those of the final *I*2 models. Although the major observed intensities were covered well, discrepancies at minor features, especially at lower angle, led to the conclusion that these alternative *A*2 models are incorrect.

Eventually, in space group *I*2 structural models could be refined for β'_1-2 PEP, β'_1-2 PSP, β'_1-2 PPE and β'_1-2 PPS. The [1-2] conformation worked out well for PEP and PSP. In PPE, however, this conformation led to unacceptable bumping problems (i.e. opposing molecules having contact distances which are to short) at the methyl end-plane interface. A [3-2] conformation did not solve this problem and even had an empty space between the aligned *sn*-2 chains. Analogous to the single-crystal structure of PPM (Sato *et al.*, 2001), combinations of two PPE molecules with different conformations, [2-1] and [2-3], were tested, but these models were also improbable owing to bumping problems at the methyl end-plane. Only with conformations [2-1] and [2-3] for β'_1-2 PPE were plausible structural models found. The slightly lower R_p value of the final [2-3] PPE model suggests this to be the more probable solution. The saturated analogue PPS showed the same conformational preference: the [2-1] model had a bumping problem and a void at the methyl end-plane. Therefore, the choice for the [2-3] PPS model was obvious and in line with the findings for PPE.

5.4.1.2 β'_0-2 PSS

Unlike the β' patterns of PEP, PSP, PPE and PPS discussed above, in the case of β'_0 -2 PSS the reflections (31ℓ) for ℓ = odd were observed, thus excluding the space group *I*2 as a potential solution. Although, eventually, in space group *C*2/*c* a structural model was obtained, its correctness was questioned because of the monoclinic β angle that is close to 90°. After testing orthorhombic space groups with an 8-fold general position, possible models were obtained only in $C222_1$ and *Pbna*. The latter was dismissed because of a 270 Å^3 void at the methyl end-plane. The $C222_1$ model refined to a final R value that is 1% higher than that of the *C*2/*c* model. Therefore, the latter is taken as the more probable structure solution.

In Table 5.3 the long spacings and strong fingerprint lines of the currently known polymorphs of PEP, PSP, PPE, PPS and PSS are listed together with the temperature $T_{\text{data coll}}$ (in K) at which the data have been collected. Anisotropic thermal properties predominantly influence the position of the strong fingerprint line with the smallest *d* value (see below; van Mechelen *et al.* 2006b and 2008) and this should be taken into account when comparing the data from Table 5.3 with literature data that have been collected at other temperatures. It should also be kept in mind that the positions of diffraction maxima can be shifted because of axial divergence and, in case of Bragg-Brentano reflection geometry, small sample displacement errors.

Although the characteristic *d* values for long spacings and fingerprint lines listed in Table 5.3 agree rather well with the limited literature data available (Lutton *et al*., 1948; Lutton, 1950; Lutton & Fehl, 1970; Elisabettini *et al.,* 1998), some discrepancies can be discerned. The long spacings of PEP and PPE of Elisabettini *et al*. (given hereafter between parentheses) are systematically longer than ours: differences of 1-2 Å are found for β'_1-2 PEP (44 Å), β'_1-2 PPE (44 Å) and α PPE (48 Å) but even up to 3-4 Å for α PEP (48 Å), β'_2-2 PEP (47 Å) and β'_2-2 PPE (46 Å). The larger long spacings of Elisabettini *et al*. may be explained by larger axial divergence, by sample displacement error (because in the reflection geometry they used the positioning of the sample is very critical for accurate low-angle positions), and a lower resolution that may have hidden the presence of a residue of the α polymorph. Presumably, the resolution of the data used by Elisabettini *et al.* was too low to observe (resolved) long spacings of the α and β'_2-2 polymorphs. The resolution of our time-resolved XRPD transmission geometry data was just high enough to establish the presence of both the α and the β'_2 long spacings, with the former being a clear shoulder of the latter. In the fingerprint area it is difficult to detect a broad α peak in presence of β'_2-2 peaks that are also broad.

The β-2 long spacings of PSP, PPE and PPS are smaller than those of the β'_1-2 polymorphs while for PEP and PSS they are longer. An explanation for this difference could be the relatively high $T_{\text{data coll}}$ of β'_1-2 PEP and β'_1-2 PSS.

The (600) is the highest-angle strong-intensity reflection in most of the β'_1 patterns but its position has been shifted remarkably in β'_1-2 PSP (Fig. 5.3). This shift is attributed to the considerably lower $T_{\text{data coll}}$ (250 K) of PSP, compared with the 297 K of the other samples, and this led to an anisotropic shrinkage of the unit-cell parameters that mainly affected the middle-sized unit-cell axis.

Table 5.3 *d* values of long spacings and strong fingerprint lines (both in Å) of polymorphs of PEP, PSP, PPE, PPS and PSS. X-ray data collected at $T_{\text{data coll}}$ (K).

TAG	α	$T_{\text{data coll}}$	β'_2-2	$T_{\text{data coll}}$	β'_1-2	$T_{\text{data coll}}$	β'_0-2	$T_{\text{data coll}}$	β-2	$T_{\text{data coll}}$
PEP	44.3 (vs)	296	43.1 (vs)	296	42.4 (vs)	324	-		43.3 (vs)	296
	4.14 (m)		4.32 (m)		4.34 (m)				4.59 (s)	
			4.17 (s)		4.19 (s)				4.55 (ms)	
			4.00 (m)		4.02 (w)				4.45 (w)	
			n.d. (w)		3.84 (m)				4.0 (w)	
									3.83 (ms)	
									3.74 (ms)	
PSP	44.7 (vs)	295	43.4 (vs)	316	42.8 (vs)	298	-		41.4 (vs)	296
	4.12 (m)		4.30 (ms)		4.32 (ms)				4.59 (s)	
			4.17 (s)		4.17 (s)				4.55 (s)	
			4.04 (m)		4.00 (m)				4.45 (m)	
			3.84 (w)		3.77 (m)				3.97 (w)	
									3.80 (ms)	
									3.72 (s)	
PPE	47.1 (vs)	296	43.5 (vs)	308	43.1 (vs)	296	-		41.9 (vs)	296
	4.14 (m)		-		4.40 (vw)				4.59 (s)	
			overlapping		4.37 (w)				4.55 (ms)	
			broad		4.28 (ms)				4.46 (vw)	
			fingerprint		4.23 (ms)				3.87 (ms)	
			peaks		4.13 (m)				3.74 (m)	
			-		4.08 (m)				3.63 (w)	
			3.9 (m)		3.82 (s)					
PPS	47.7 (vs)	295	43.8 (vs)	324	43.5 (vs)	298	-		42.3 (vs)	296
	4.11 (m)		-		4.37 (w)				4.59 (s)	
			overlapping		4.27 (s)				4.56 (s)	
			broad		4.24 (s)				3.83 (ms)	
			fingerprint		4.12 (ms)				3.69 (ms)	
			lines		4.08 (ms)					
			3.84 (m)		3.78 (s)					
PSS	48.3 (vs)	295	45.1 (vs)	328	44.7 (vs)	333	44.7 (vs)	295	45.7 (vs)	293
	4.11 (m)		4.31 (ms)		4.35 (m)		4.51 (vw)		4.62 (s)	
			4.21 (s)		4.22 (s)		4.47 (vw)		4.55 (s)	
			4.07 (ms)		4.06 (m)		4.38 (w)		4.44 (vw)	
			3.86 (m)		3.85 (ms)		4.32 (w)		3.96 (w)	
							4.19 (ms)		3.84 (ms)	
							4.11 (ms)		3.73 (w)	
							4.03 (w)		3.66 (ms)	
							3.77 (s)			

5.4.3 Phase transitions and stability of polymorphs

The T_m and phase-transition temperatures obtained with the constant heating-rate experiments (Table 5.1) show that the symmetric PEP and PSP are β' stable. The asymmetric PPE, PPS and PSS are β stable although the difference in T_m between the highest melting β' form and the β form is very small for PSS and PPE. The similar melting points explain why a β_1'-2 to β-2 conversion was not observed for PSS and PPE within a week of annealing the β_1'-2 2 K below its melting point. For PPS the conversion did occur and was completed in one day.

With respect to the reproducibility of β' melting points of mono-acid TAGs determined with DTA, Lutton & Fehl (1970) reported that 'under the best conditions' an error of ±1 K can be achieved, although stabilization and sample preparation also affect the melting points. Variations in T_m's up to 3 K have been attributed to these phenomena (Lutton *et al.*, 1948). The melting and phase-transition points listed in Table 5.1 are expected to have an uncertainty of the same order. An optimal stabilization was not feasible for many of the metastable polymorphs because of potential phase transitions.

The heating rate used must be regarded as a parameter that influences the observed temperatures. For example, Elisabettini *et al*. (1998) obtained for PEP with DSC (heating 5 K min^{-1}) a much higher β'_2-2 to β'_1-2 transition temperature (320 K) than the 303 K obtained with our XRPD at 0.5 K min^{-1}. The notion that even a modest heating rate may lead to a significant overshoot of the phase-transition temperature implies that one should be careful with conclusions about melting or phase-transitions temperatures that have not been measured under the same experimental conditions.

5.4.3.1 The $\alpha \rightarrow \beta'_2$ phase transition

The $\alpha \rightarrow \beta'_2$ transition is difficult to analyze with time-resolved XRPD because of the overlap at low angles and in the fingerprint area. With DSC (0.5 K min^{-1}) the symmetric TAGs (PSP and PEP) show no significant melting peak before the $\alpha \rightarrow \beta'_2$ transition. However, in case of the asymmetric TAGs (PPE, PPS and PSS) the formation of β'_2 is clearly preceded by the melting of the α phase (DSC data not shown). This is in line with the results of Elisabettini *et al.* (1998) who concluded from 5 K min^{-1} DSC traces that in PEP the $\alpha \rightarrow \beta'_2$ transition is a solid-state transition (no melting peak) whereas in PPE a melt is involved. Apparently, for asymmetric TAGs the $\alpha \rightarrow \beta'_2$ transition is more complicated than for symmetric TAGs, suggesting larger conformational changes in the former.

5.4.3.2 The $\beta'_2 \rightarrow \beta'_1$ phase transition

In Fig. 5.4 a selection of diffraction patterns shows the melt and crystallization experiment of PSS. The determined melt and phase-transition temperatures, including the β'_2-2 $\rightarrow$ β'_1-2 transition point, are marked at the right-hand side of the patterns. The virtually equal positions of the β'_1-2 and β'_2-2 fingerprint maxima, within the accuracy and resolution of the data, and the growth of sharper β'_1-2 peaks at the centres of the broad(er) β'_2-2 diffraction maxima suggests that the β'_1-2 is just a higher-crystalline form of the β'_2-2 polymorph. The close structural relation between the β'_2-2 and β'_1-2 polymorphs, also suggested by Kellens *et al.* (1990), and the related, small amount of energy involved in such a transition may explain the difficulty in locating it in the DSC trace. The systematically lower intensity of the (600) reflection in the β'_2-2 patterns compared with the β'_1-2 (Fig. 5.5) may be an indication for a type of disorder in the direction of the *a* axis in β'_2-2 polymorphs.

The stability of the β'_2-2 differs drastically between TAG groups and also depends on the thermal treatment. When slowly heating (0.5 K min^{-1}), the transition of the least stable β'_2-2 to the β'_1-2 starts 2 K (4 min.) after the former's appearance (Table 5.1, PSP and PPS). For PSS and PPE this interval is 7 K and for PEP even 11 K. This suggests that an exchange of S by E considerably delays the appearance of β'_1-2 and thus stabilizes the β'_2-2 polymorph. While the existence of the β'_2-2 polymorph is difficult to prove for a mono-acid trisaturated TAG like SSS because of instability (Simpson & Hageman, 1982), substitution of one (*n*) chain by a longer (*n* + 2) one stabilizes the β'_2-2 polymorph and substitution by a shorter (*n* - 2) chain stabilizes it even more.

5.4.3.3 Stability of β'_1-2

The gap between the β'_2-2 $\rightarrow$ β'_1-2 transition point and the melting point of the β'_1 polymorph is different for symmetric *versus* asymmetric TAGs. For the asymmetric samples the β'_1 melts within 9 K (18 min) after its formation, while the symmetric PEP and PSP melt 17 K (34 min) and 24 K (48 min), respectively, above their appearance temperature. From this considerable difference in “lifetime” it can be concluded that asymmetry destabilizes the β'_1-2 polymorph, presumably as a result of the different conformation. In going from PSP to PEP the β'_1-2 lifetime drops by 7 K (14 min) but in the asymmetric TAGs the exchange of S by E

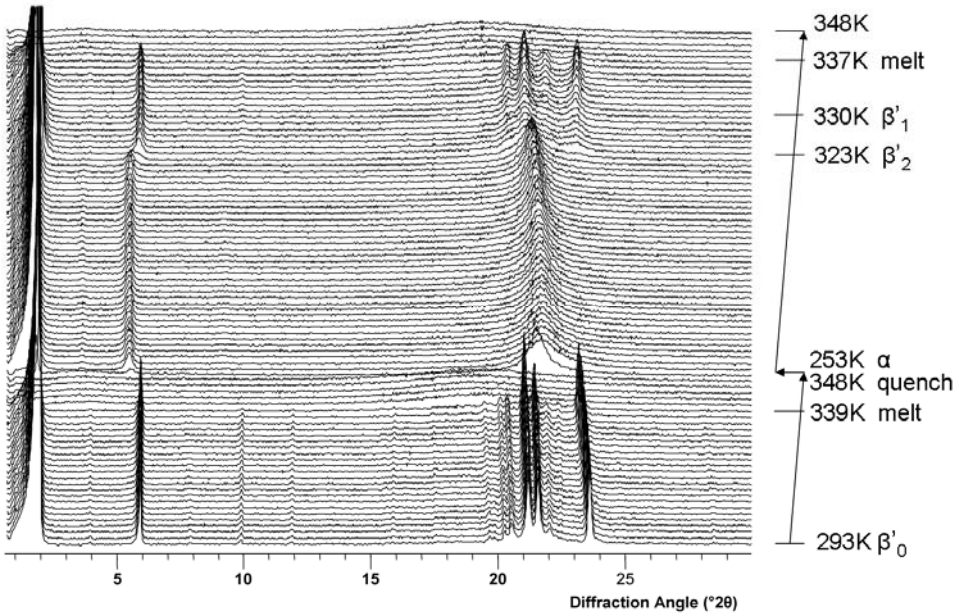

Fig. 5.4 Melting and recrystallization of PSS polymorphs: from bottom to top: the starting polymorph β'_0 melts and after quenching (-30 K min^{-1}) and subsequent heating (0.5 K min^{-1}) α, β'_2 and β'_1 appear and melt. Relevant temperatures are listed to the right of the graph.

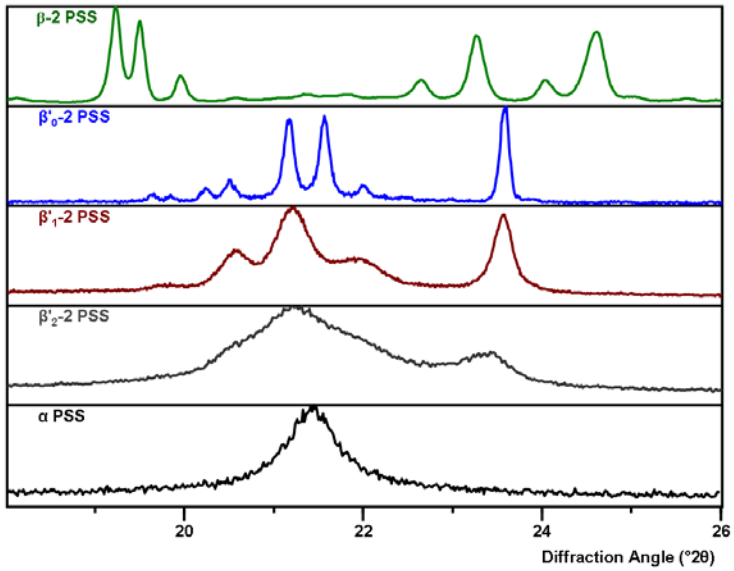

Fig. 5.5 Fingerprint area of the polymorphs of PSS.

does not seem to have a significant lifetime influence on the β'_1-2 phase. Only the absolute values of the β'_1-2 melting points show the influence of an exchange of S by E since it causes a considerable drop of the melting point, just as for the β melting points.

5.4.3.4 β'_0-2 PSS

In older literature PSS has been reported to be β' stable, just like PSP (Lutton *et al.*, 1948), but also to have equally stable β' and β polymorphs (Lutton, 1950). With our crystallization procedure and heating the sample just above the β'_2 to β'_1 conversion temperature, a β'_1 polymorph was initially obtained. Surprisingly, after storage in the lab for several weeks at room temperature ($T \approx 294$ K), all the prepared capillaries appeared to contain a novel β'-type polymorph (diffraction pattern at the bottom of Fig. 5.2) that differed from the β'_1-2. The novel β'-type PSS polymorph will be denoted as β'_0-2 because its melting point (339 K) is higher than that of the β'_1-2 polymorph (336 K). A melt and recrystallization experiment carried out with this novel polymorph (Fig. 5.4) delivered a pattern that resembles those of the β'_1-2 polymorphs shown in Fig. 5.2.

Fig. 5.5 gives an overview of the fingerprint areas of all known polymorphs of PSS. Although the β'_0-2 melting point almost equals that of the β-2 polymorph, the β'_0-2 polymorph cannot be mistaken as a β-2 polymorph because the β'_0-2 XRPD pattern clearly lacks the characteristic β-2 reflections between 19 and 19.5 °2θ (upper trace Fig. 5.5). Also, the characteristic β' bend conformation (see below) and the β'-typical (600) reflection at 23.6 °2θ classifies it as a β' family member.

The T_m values of the β'_0-2 and the β-2 polymorphs (Table 5.1), determined using two different samples from the same PSS batch, are equal within the accuracy of the temperature measurement and suggest an equal stability. A time- and temperature-resolved diffraction experiment has been carried out with a third PSS capillary sample, taken from the same batch and prepared in the same way as the other two. Unlike the other two samples, this third sample contained β'_0 but also a small amount of β. Upon heating this sample with 0.5 K min^{-1} the diffraction patterns show that the β'_0 melts 1.5 - 2 K before the β, so it is concluded that PSS is not β_0'-2 but β-2 stable.

Questions concerning the precise conditions under which the β'_0-2 and the β-2 crystallize, and whether a tempering process may stimulate this, remain as yet unanswered. Repeatedly partial melting of β'_1-2 PSS at 336 K and followed by

cooling to 335 K sharpened the β'_1-2 peaks in the XRPD pattern, but did not induce a conversion to β'_0-2, neither to β-2. After 3 months storage of β'_1-2 at 330 K a small amount of β'_0-2 was detectable. These experiments demonstrate the influence of sample history on T_m values and show that one should take care in drawing conclusions from experimentally obtained thermal data, even if the samples originate from the same batch.

5.4.4 Packing and methyl end-plane

5.4.4.1 β'_1-2 PEP, β'_1-2 PSP, β'_1-2 PPE and β'_1-2 PPS

In all the β'_1-2 structures discussed in this publication the conformation of the chair-shaped molecules shows the typical β' bend of ~ 130° between back and back leg of the chair (the same as in van Langevelde *et al*., 2000; Sato *et al.*, 2001) Also, in all the β' structures the molecules are packed with seats facing each other, but being slightly tilted, while the back of the one molecule is adjacent to the front

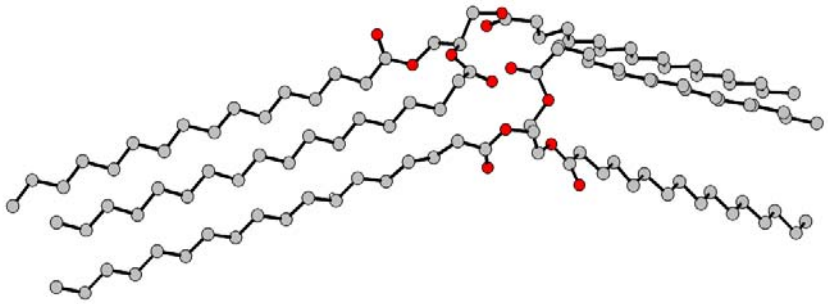

Fig. 5.6 Pair of PSS molecules with facing seats.

leg of the other one (Fig. 5.6). The legs of the one (upper) molecule (Fig. 5.6, left-hand side) are packed in the same layer as the back of the other (lower) molecule, but the legs of the lower molecule and the back leg of the lower molecule (Fig. 5.6, right-hand side) are packed in another, different layer than its front leg and the back of the upper molecule. The pairs of molecules form 'two-pack' layers with a double-chain length thickness. The unit cell of the β'_1-2 structure contains two of such 'two-packs' that are related to each other by a (½,½,½) translation. The bends in the molecules point in the same direction, as a result of which the 'two-packs'

approach each other at the methyl end-plane with the same angle as the bend in the molecules (Fig. 5.7). The methyl end-groups at one side of the interface between the 'two-packs' point in between two methyl end-groups of the adjacent 'two-pack' (Fig. 5.7b). The view along the *b* axis shows a difference between the packing of

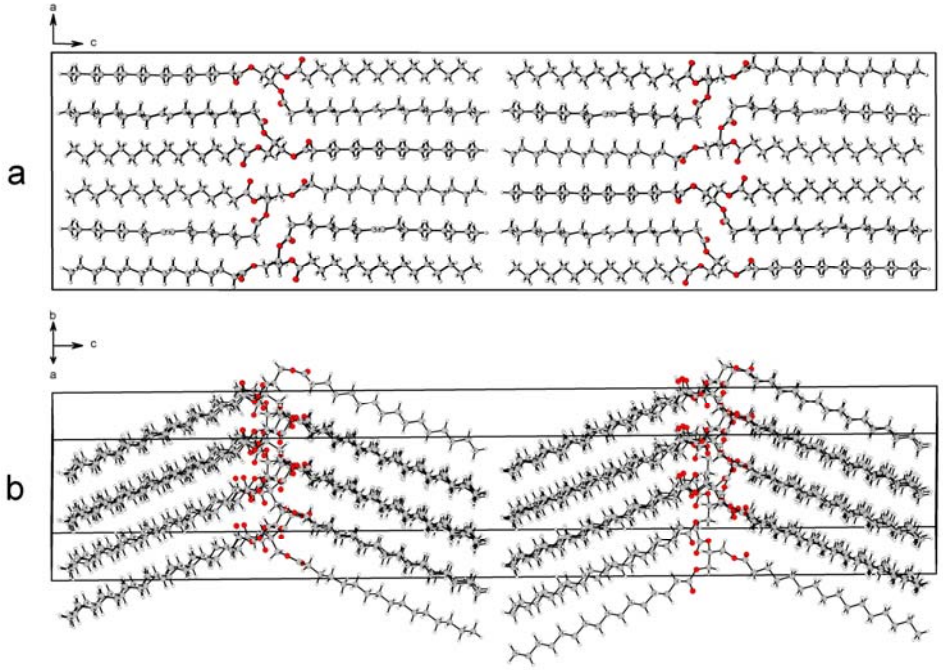

Fig. 5.7 Packing of β'_1-2 PEP, (*a*) view parallel to the *b* axis, (*b*) view parallel to [130].

the symmetric and asymmetric β'_1-2 structures: In the symmetric structures the chains at the methyl end-plane are aligned in projection on the *ac* plane (Fig. 5.7a) whereas in the asymmetric structures the chain ends of one 'two-pack' point between two other chains of the neighbouring 'two-pack' (Fig. 5.8).

The precise location of the seat of the chair-shaped molecules in between the dominating columns of electron density of the zigzag chains is a point that deserves extra attention. If opposing chair seats at the front-leg side bump, the seat position is likely to be incorrect. The solution to this bumping problem is similar to that described for β-2 structures: rotation of the seat plus front leg along the back leg axis until the front leg coincides with a neighbouring column of electron density (van Mechelen *et al*., 2006b).

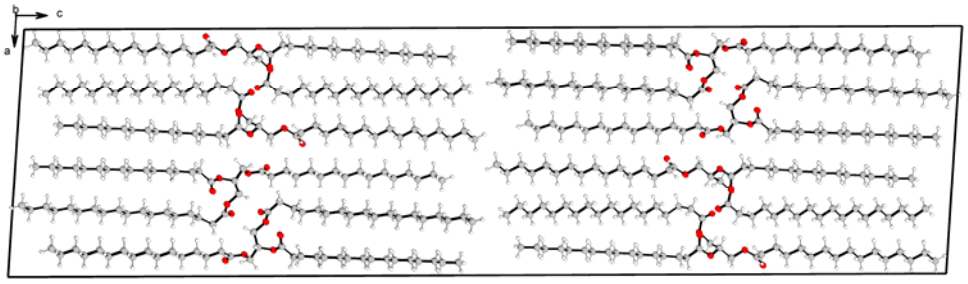

Fig. 5.8 Packing of [2-3] β'_1-2 PPS: view along the *b* axis.

However, at the given resolution of the data two serious ambiguities exist in the packing of the β'_1 structures of PPS, PPE, PSP and PEP. The first is the position of the methyl end-plane. When the molecules are shifted by *c*/4 and rotated by 180° along the direction of the *c* axis, a packing can be realized that fills the columns of electron density of the parallel parts of the acyl chains but with the methyl end-plane and the glycerol zone interchanged and having the seat at a different position. The *R* values for both packings are virtually the same so from the XRPD data no choice can be made for the methyl end-plane position. This ambiguity may be solved by comparing with the single-crystal data of β'_1 CLC. At room temperature this crystal structure is orthorhombic but at lower temperatures β'_1 CLC becomes monoclinic. Since this orthorhombic to monoclinic transition is reversible, it is likely that no changes are involved other than small shifts and rotations. The similarity between the powder pattern of the monoclinic β'_1 CLC and the β'_1 patterns of the present study supports a structural equivalence and for this reason the methyl end-plane position has been taken as conforming to that in β'_1 CLC (van Langevelde *et al.,* 1999).

The second ambiguity is the orientation of the second molecule in the asymmetric unit of the *I*2 structure. Each molecule forms a seat-facing pair with a symmetry copy of itself. When the lower left quarter of the unit cell (Fig. 5.7a) is filled by a molecule pair of molecule (1), the upper-left quarter is filled by molecule (2). When molecule (1) has approximately the proper configuration molecule (2) may be obtained in two ways: by shifting a copy of molecule (1) by *a*/2 relative to molecule (1) (option 1), or by shifting a copy of molecule (1) by *a*/2 plus an additional 180° rotation with respect to an axis at (3*a*/4, *c*/4) perpendicular to the *ac* plane (option 2). After optimisation by *FOX*, both molecule combinations lead to structure solutions that differ mainly in the position of the seat of the second molecule. Just as with the previous ambiguity, the single-crystal data of β'_1 CLC has been used to select the second option. The seat-position ambiguity is not unique for structure solution of TAGs from powder diffraction data. Even in the

single-crystal structure solution of β'_1 CLC, the seat position was a problem (private communication) and only from a $2mF_0$ - DF_{calc} electron density map it could be established unambiguously (van Langevelde *et al.,* 2000).

5.4.4.2 β'_0-2 PSS

The unit cell of the β'_0-2 structure of PSS also contains two 'two-packs', but these are related by an inversion centre. This makes the bends in the two 'two-packs' point in opposite directions whereas the chains of the approaching 'two-packs' at the methyl end-plane are not inclined but parallel and aligned (Fig. 5.9). The methyl end-plane of the 'two-packs' is stepped (Fig. 5.9a) and can be denoted as a ⟨2-2⟩ interface as the *sn*-2 chains of neighbouring 'two-packs' are in line, analogous to the β-2 polymorphs of these TAGs (van Mechelen, *et al.,* 2008).

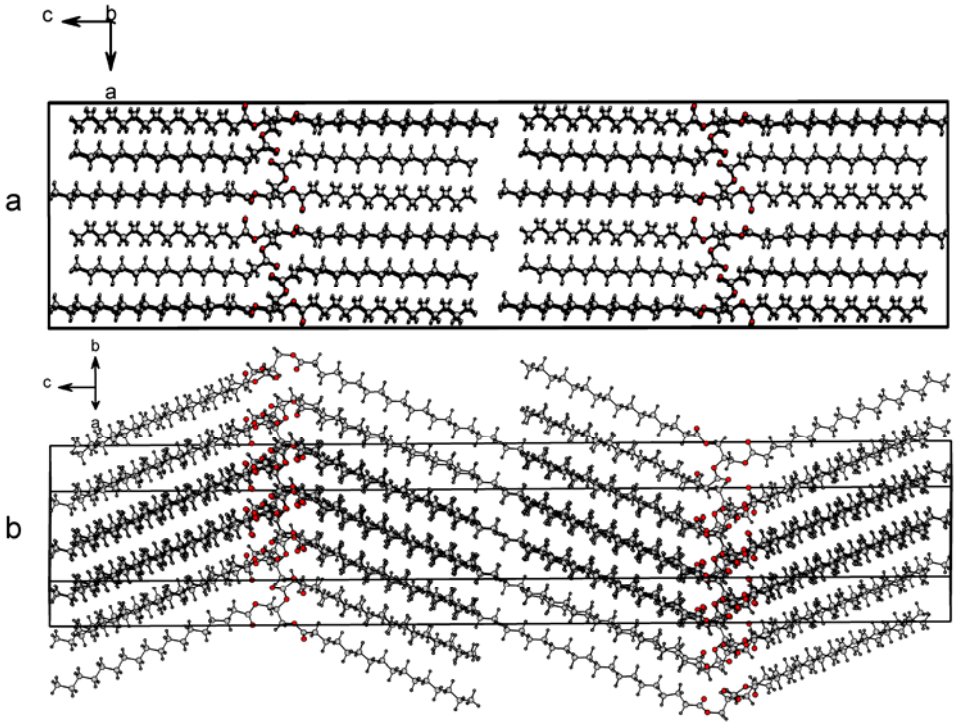

Fig. 5.9 Packing of β'_0-2 PSS, (*a*) view parallel to the *b* axis, (*b*) view parallel to [310].

5.4.5 Comparison of β′ structures

The fingerprint area of the diffraction patterns of all the β'-2 structures is dominated by the (600) and (31ℓ) reflections (Fig. 5.3). The lattice planes (600), (318) and (31-8) are related to the most intense fingerprint diffraction maxima because of their orientation relative to the chain packing (Fig. 5.10). Based on FT-IR measurements on micro crystals, Yano *et al*. (1997) suggested an $O_\perp$ subcell for

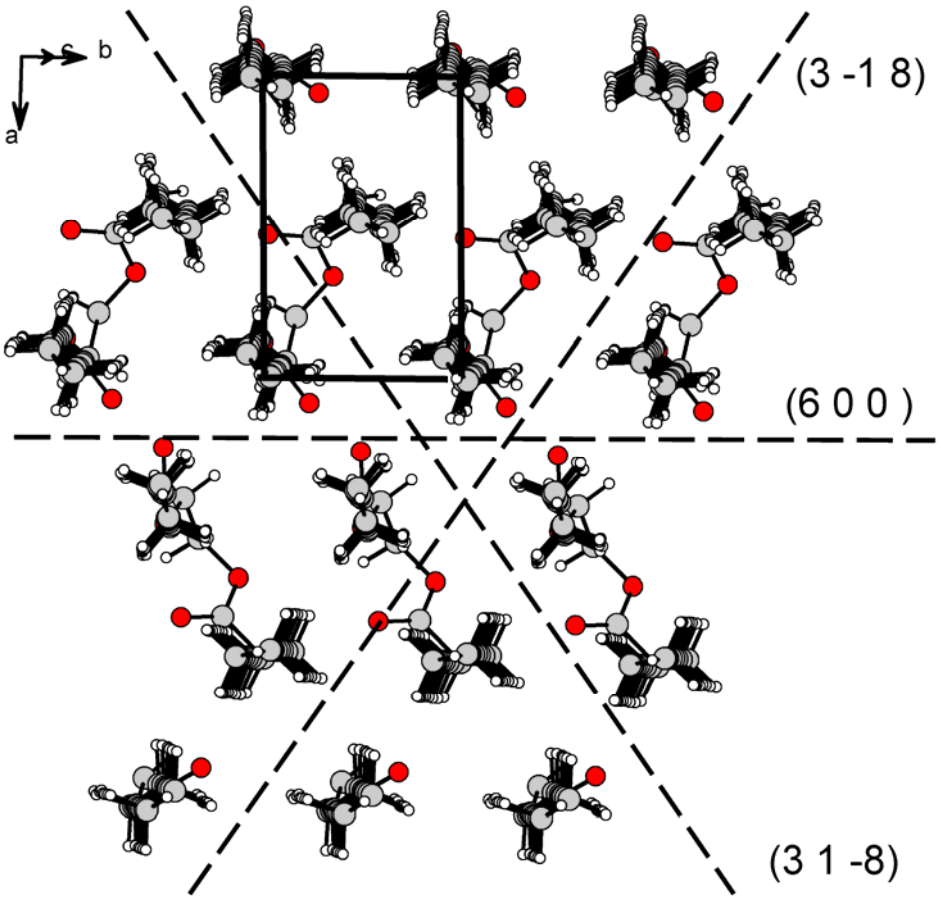

Fig. 5.10 View parallel to the chain direction of half a β'_1-2 PSP 'two-pack'. Dotted lines mark the orientation of the lattice planes corresponding to the main finger print lines. Solid lines: the $O_\perp$ subcell in line with the one present in β'_1-2 CLC.

the β'_1-2 structure. This subcell is found in the single-crystal structure of β'_1-2 CLC (van Langevelde *et al.,* 2000) and does not conflict with the data of the β'_1-2 structures of this paper. However, at the resolution to which the β'_1 TAGs diffract (not beyond 3 Å), the orientation of the zigzag planes of the acyl chains, and thus the subcell, cannot be established unambiguously. Since the same problem applies to β'_0-2, it is obvious that the usefulness of the subcell is quite limited.

The 'two-packs' in the β' structures can be described as two stacked dimers that each consist of two symmetry-related molecules. The dimeric symmetry (2_1 axis parallel to the *b* axis) is the same in all cases but the stacking of the dimers can be different. In the β'_1-2 structures of this work the dimers in the 'two-packs' are not symmetry related, in the orthorhombic β'_1-2 (room-temperature) crystal structure of CLC (van Langevelde *et al.,* 2000), they are symmetry related by a *b* glide perpendicular to the *a* axis and in the β'_0-2 of PSS the dimers are related by a (½,½,0) translation.

The symmetric and asymmetric β'_1-2 TAGs appear to have different conformations, the former a [1-2] and the latter a [2-3]. This difference in conformation suggests a relation to their different behaviour at the $\alpha \rightarrow \beta'_2$ transition. For the symmetrical group that does not exhibit a clear α melting it seems likely that the [1-2] β' conformation is maintained from the α form. However, the asymmetric TAGs do show α melting and this may be related to the change from the [1-2] conformation to the [2-3] conformation.

Judging from the β'_1-2 models and the β'_0-2 PSS model, the transition of β'_1-2 PSS to β'_0-2 PSS has to involve an inversion of the orientation of every other 'two-pack'. This symmetry relation between the 'two-packs' in β'_1-2 *versus* β'_0-2 is similar to that found for the 'three-packs' in the β_2-3 *versus* β_1-3 polymorphs of *cis*-mono-unsaturared TAGs: in the lower-melting polymorph the 'three-packs' are related via a translation (½,½,½) while in the higher-melting one they are related by a centre of symmetry (van Mechelen *et al*., 2006b).

It should be noted that apart from the β'_2-2, β'_1-2 and β'_0-2 discussed in the present paper also other types of β' structures do exist. For example, a crystal structure of a β'-2 polymorph of PPM has been solved from single-crystal data (Sato *et al.*, 2001). This asymmetric β'-2 structure has two molecules in the asymmetric unit, just like the *I*2 structures of the present paper, but the two molecules have different conformations, a [2-1] and a [2-3] that together form a seat-facing pair. A (calculated) powder diffraction pattern clearly shows that this compound belongs to a different class of β'-2 structures because the reflection (600) is missing. It seems relevant to note that the β'-2 PPM single crystal was crystallized from *n*-hexane whilst the β' polycrystalline material used for the present work was obtained without solvent.

5.4.6 Comparison of β′ and the β structures

The *β′*-2 polymorphs presented in this paper are either in a [1-2] conformation (PEP, PSP, PSS) or in a [2-3] conformation (PPE, PPS), and have a bend between the back and the back leg. It is noted that in all cases the seat of the chair is a C18 chain (E or S), apparently a conformation that is energetically favourable, and this may explain the [2-3] conformation of PPE and PPS that both have a shorter *sn*-2 chain.

In contrast, the *β*-2 polymorphs of all these materials (see Part III of this series; van Mechelen *et al*., 2008) are all in a [1-3] conformation. In this conformation the back and the back-leg of the seat, formed by the *sn*-1 and *sn*-2 chains, are lined up and the parallel planes of the zigzag chains form a triclinic subcell. The different molecular conformations in *β′*-2 *versus β*-2 imply that rather complicated changes are required in the transition from *β′*-2 to *β*-2 and this may explain the difficulty in getting a *β* phase. The symmetric PEP and PSP are *β′* stable and since the *β*-2 of PSP and PEP melt at lower temperatures, a *β′* to *β* conversion cannot be observed. It seems likely that this *β* phase can be obtained only if the melt-mediated *β′*-2 can be avoided, *e.g.* by crystallization from a solvent (Lutton & Hugenberg, 1960). The latter authors reported that *β*-2 PSP transforms into β'_1-2 at 338 K *via* the melt. The melting indicates a change in conformation and/or packing, in line with the structural differences we determined. The asymmetric PPS and PSS, and probably also PPE, are *β*-2 stable, as shown from the melting points. The β'_1 to *β* conversion rate in these cases is very slow, if conversion occurs at all, so measuring the conversion with DSC is impossible. With temperature-resolved XRPD the precise conditions to stimulate the transition in a controlled and reproducible way have not been established yet.

5.5 Conclusions

The β'_1-2 structures of PSP, PEP, PPS and PPE have been solved from high resolution powder diffraction data in space group *I*2. The packing is in line with the orthorhombic single-crystal structure of β'_1-2 CLC (van Langevelde e*t al.,* 2000). The presence of two molecules in the asymmetric unit complicated the structure solution and, together with dominant-zone problems and peak overlap in the diffraction pattern, it hindered the determination of the orientation of the zigzag planes of the acyl chains. Unlike the *β*-2 structures of these compounds (van Mechelen *et al*., 2008) the symmetric and asymmetric β'_1-2 have different molecular conformations. The structure of a novel *β′* polymorph of PSS, named

β'_0-2, was solved in space group *C*2/*c*. The molecule has a characteristic β' bend conformation. Time- and temperature-dependent XRPD experiments showed that both the β'_1-2 PSS and the β'_0-2 PSS melt at lower temperatures than the β polymorph, so justify the conclusion that PSS is β stable. The difference in molecular conformation between the β'-2 polymorphs and the β-2 polymorph makes a β'-2 to β-2 solid-state transition unlikely. For the β'_1-2 structures as well as the β'_0-2, the dominant zones in the finger print area of the diffraction pattern can be correlated with the layered packing of the acyl chains.

In the case of the structure determination of *cis*-mono-unsaturated β-3 type TAGs it was shown that the diffraction data are not very sensitive to rotational freedom of zigzag chains around their longitudinal axis (van Mechelen *et al*., 2006a). This holds for the β'-2 structure of PSS in *C*2/*c*, having a single molecule in the asymmetric unit just like the β-3 structures. The rotational freedom is an even more serious problem in the β'_1-2 structures because they have two molecules in the asymmetric unit while their powder patterns do not have more independent reflections. Thus, no firm conclusions are possible about the orientation of the planes of the zigzag chains on the basis of non-atomic resolution XRPD data alone.

5.6 Acknowledgements

The authors thank Unilever Research Vlaardingen for the PSP sample. The authors acknowledge the ESRF (Grenoble, France) for providing the facilities to perform the synchrotron diffraction experiments and they thank W. van Beek of the Swiss-Norwegian CRG beamline BM01b for his valuable help during the experimental sessions. The authors also thank E. Sonneveld (UvA) for his help in data collection during the experimental session at BM01b. Shell Research and Technology Centre Amsterdam is acknowledged for making the DSC cell available. The investigations have been supported by the Netherlands Foundation for Chemical Research (NWO/CW) with financial aid from the Netherlands Technology Foundation (STW; project 790.35.405). The members of the User Committee of this project are thanked for stimulating discussions and continuous interest.

5.7 References

Dollase, W. A. (1986). *J. Appl. Cryst*. **19**, 267-272.

Elisabettini, P., Lognay, G., Desmedt, A., Culot, C., Istasse, N., Deffense, E. & Durant, F. (1998). *J. Am. Oil Chem. Soc*. **75**, 285-291.

Favre-Nicolin, V. & Cerný, R. (2002). *J. Appl. Cryst*. **35**, 734-743.

Ghotra, B.S., Dyal, S.D. & Narine, S.S. (2002). *Food Res. Int.* **35**, 1015-1048.

Gibon, V., Blanpain, P., Durant, F. & Deroanne, Cl. (1985). *Belg. J. Food Chem. Biotechn.* **40,** 119-134.

Kellens, M., Gibon, V., Hendrix, M. & De Greyt, W. (2007). *Eur. J. Lipid Sci. Technol.* **109**, 336-349.

Kellens, M., Meeussen, W. & Reynaers, H. (1990). *Chem. Phys. Lipids* **55**, 163-178.

Langevelde, A.J. van, van Malssen, K.F., Driessen, R., Goubitz, K., Hollander, F.F.A., Peschar, R., Zwart, P. and Schenk , H. (2000). *Acta Cryst.* B**56** , 1103-1111.

Langevelde, A. van, van Malssen, K., Sonneveld, E., Peschar, R. & Schenk, H. (1999). *J. Am. Oil Chem. Soc.* **76**, 603-609.

Larson, A.C. & Von Dreele, R. (1987). *GSAS*. Report No. LA-UR-86-748. Los Alamos National Laboratory, New Mexico, USA.

Laugier, J. & Bochu, B.(2001). *Chekcell*; http://www.inpg.Fr/LMPG.

Le Bail, A. (2004). *Powder Diffr.* **19,** 249-254.

Lutton, E.S. (1950). *J. of Am. Oil Chem. Soc*. **27**, 276-281.

Lutton, E.S. & Fehl, A.J. (1970). *Lipids* **5**, 90-99.

Lutton, E.S. & Hugenberg, F.R. (1960). *J. Chem. Eng. data* **5**, 489-490.

Lutton, E.S., Jackson, F.L. & Quimby, O.T. (1948). *J. Am. Chem. Soc.* **70**, 2441-2445.

March, A. (1932). *Z. Kristallogr*. 81, 285-297.

Mechelen, J.B. van , Peschar, R. & Schenk, H. (2006a). *Acta.Cryst*. B**62**, 1121-1130.

Mechelen, J.B. van, Peschar, R. & Schenk, H. (2006b). *Acta.Cryst*. B**62**, 1131-1138.

Mechelen, J.B. van, Peschar, R. & Schenk, H. (2008). *Acta.Cryst*. B**64,** 240-248.

Sato, K., Goto, M., Yano, J., Honda, K, Kodali, D.R. & Small, D.M. (2001). *J. Lipid Res.* **42**, 338-345.

Simpson, T.D. & Hageman, J.W. (1982). *J. Am. Oil Chem. Soc.* **59**, 169-171.

Sreenivasan, B. (1978). *J. Am. Oil Chem. Soc.* **55,** 796-805.

Timms, R.E. (2005). *Eur. J. Lipid Sci. Technol.* **107**, 48-57.

Valenzuela, A. & Morgado, N. (1999). *Bio. Res.* **32**, 273-287.

Watanabe, A., Tashima, I., Matsuzaki, N., Kurashige, J. & Sato, K. (1992). *J. Am. Oil Chem. Soc*. **69**, 1077-1080.

Wiedermann, L.H. (1978). *J. Am. Oil Chem. Soc.* **55**, 823-829.

Yano, J., Kaneko, F., Kobayashi, M., Kodali, D.R., Small, D.M. & Sato, K. (1997). *J. Phys. Chem. B* **101**, 8120-8128.

5.8 Appendix

Rietveld refinement results of β'-2 structures

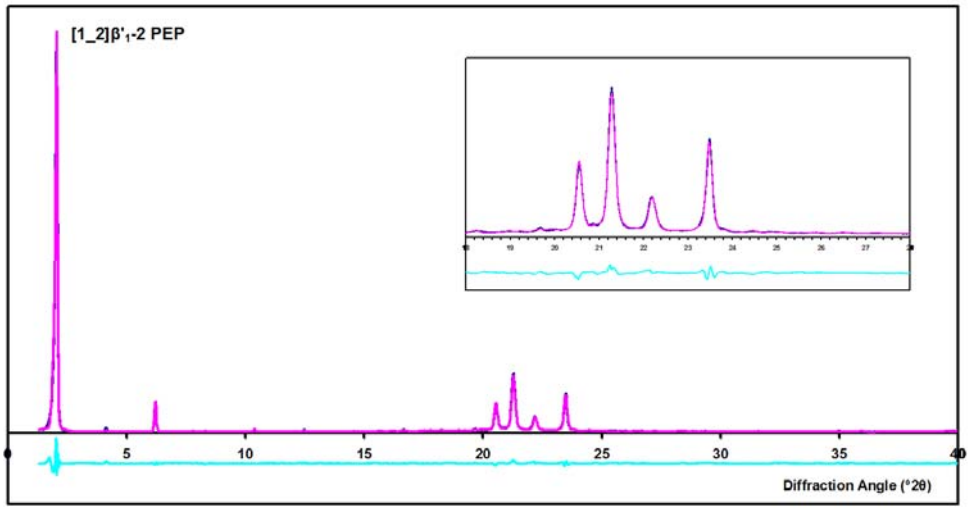

Fig. 5.11 Rietveld refinement result of β'_1-2 PEP with difference trace of the measured and calculated patterns.

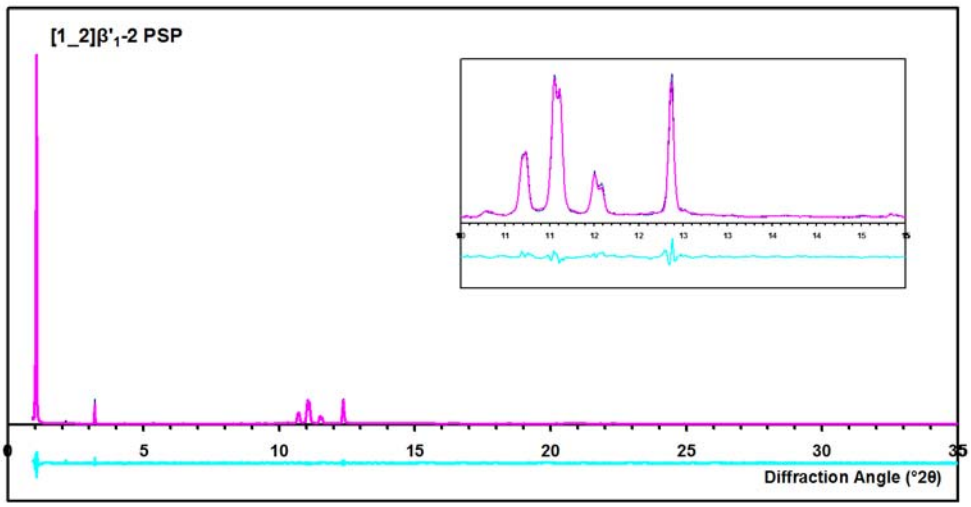

Fig. 5.12 Rietveld refinement result of β'_1-2 PSP with difference trace of the measured and calculated patterns.

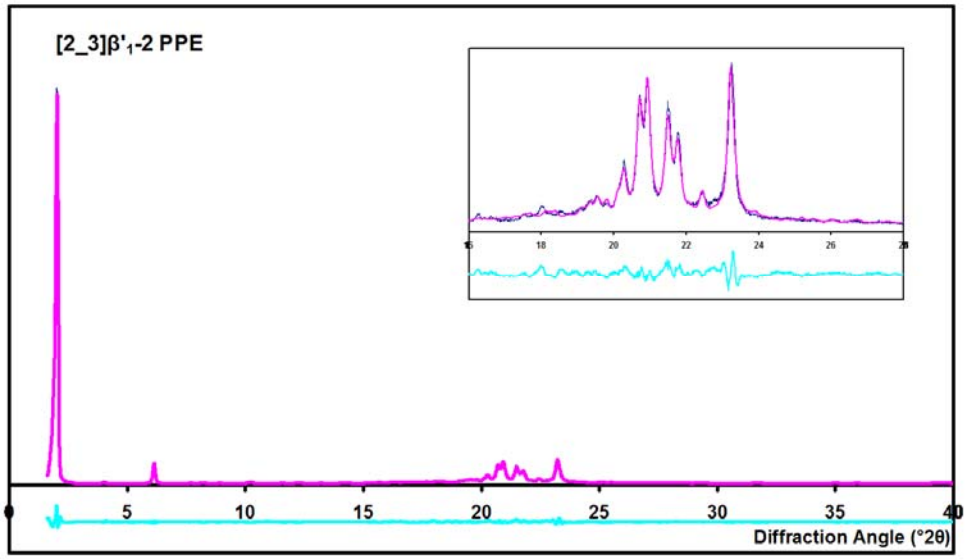

Fig. 5.13 Rietveld refinement result of β'_1-2 PPE with difference trace of the measured and calculated patterns.

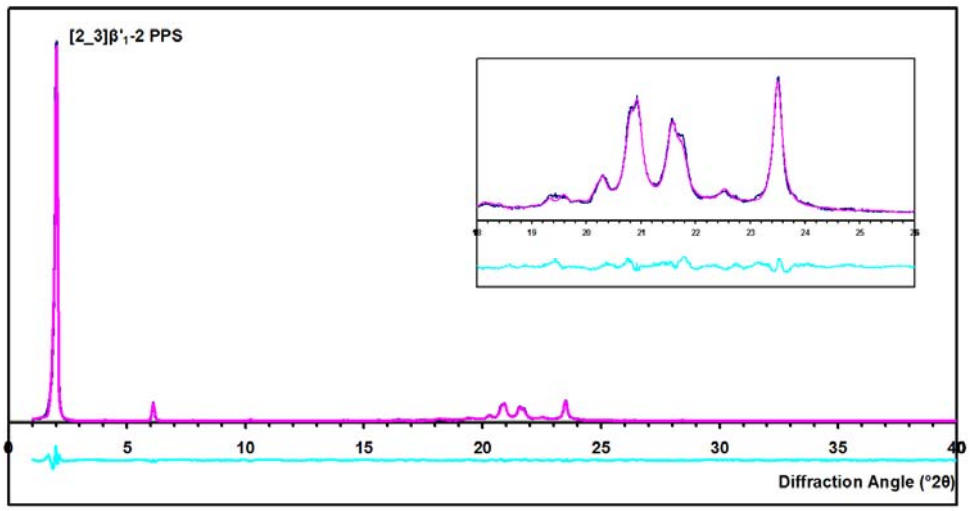

Fig. 5.14 Rietveld refinement result of β'_1-2 PPS with difference trace of the measured and calculated patterns.

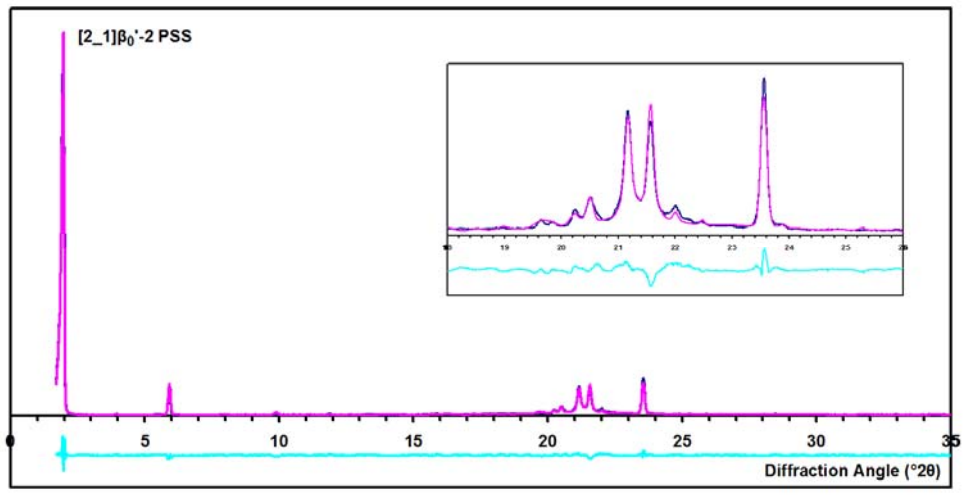

Fig. 5.15 Rietveld refinement result of β'_0-2 PSS with difference trace of the measured and calculated patterns.